ARTICLES

In-Situ Transmission Electron Microscopic Study of Perovskite-type Niobate Nanosheets under Electron-Irradiation and Heating

Fang-Fang Xu,* Yasuo Ebina, Yoshio Bando, and Takayoshi Sasaki

National Institute for Materials Science (NIMS), 1-1 Namiki, Tsukuba, Ibaraki 305-0044, Japan

Received: February 13, 2002; In Final Form: May 7, 2003

In-situ transmission electron microscopic (TEM) observation has been performed in the study of effects of electron irradiation and heating on the perovskite-type (TBA, H)$Ca_2Nb_3O_{10}$ nanosheet material. Radiation-induced migration of vacancies was found to play an important role in the generation of various structural defects under electron irradiation at room temperature. Irradiation-induced defects include loops and stacking fault pyramids (SFP). SFPs are the new structural features since they neither have been discovered in bulk perovskite materials nor have been generated as extended defects under irradiation. Extraction of interlayer molecules via thermal dynamic effects of electron illumination has produced a variety of domain boundaries including antiphase boundaries, δ-boundaries, and amorphous interfaces due to irradiation damage. The present nanosheet material has also been heated to ~500 °C during the in-situ TEM observation. Periodic antiphase domain boundary structures have been observed after heating.

Introduction

Nanosheet is a new concept in the family of nanosized materials. It shows two-dimensional crystal lattice with an ultrathin thickness.[1] Recently, nanosheets of titanates[2] and niobates[3] have been synthesized by delaminating precursor layered crystals into their elementary layers. These oxide nanosheets have been found to exhibit distinctive physicochemical properties characteristic of a semiconductor.[4] For example, the nanosheet crystallite of $Ti_{1-\delta}O_2^{4\delta-}$ ($\delta \sim 0.09$) shows a very sharp optical absorption peak which is appreciably blue-shifted relative to the band gap energy of bulk titanium oxides.[4b]

Perovskite-type niobate nanosheets with the nominal composition of (TBA, H)$Ca_2Nb_3O_{10}$ have been prepared in our present work.[5] The elementary nanosheet consists of three NbO_6 octahedral layers of perovskite structure. Perovskite-type oxides have shown a wide variety of interesting physicochemical properties such as superconductivity,[6] ferroelectricity,[7] photocatalysis,[8] and magnetoresistance.[9] Thus, the perovskite-type oxides have attracted much attention, especially in the study of effects of irradiation on their structures and properties by a variety of particles, e.g., photons,[10] ions,[11] gamma,[12] laser,[13] neutrons,[14] and electrons.[15] In this paper, we are interested in the effects of electron irradiation on the perovskite-type niobate nanosheet material and wanted to know if this specific two-dimensional nano-crystallite would exhibit radiation-induced structural features (e.g., defect structures) different from those observed in bulk perovskite materials. Transmission electron microscopy (TEM) proved to be an adequate technique for experimental studies of irradiation-induced structural features as it allows in-situ irradiation and observation.

* Corresponding author. Tel: 81-29-8513354, ext 8582. Fax: 81-29-8516280. E-mail: XU.Fangfang@nims.go.jp.

An in-situ TEM study on the effects of electron irradiation has been performed at room temperature. Both the kinematical and dynamical effects of electron irradiation on the nanosheet aggregates have been examined. Meanwhile, effects of heating on the structures of nanosheets have also been studied on a double-tilt thermal specimen holder for in-situ TEM analysis. Practical application of the nanosheet materials must be preceded by the extraction of interlayer molecules. Thus, study on the effects of the heating process is very important. The present work has shown some interesting radiation-induced and heat-induced structural features that have never been observed in bulk perovskite materials.

Experimental Section

Materials Preparation. A layered perovskite, $KCa_2Nb_3O_{10}$, was prepared by calcining mixed powders of K_2CO_3, $CaCO_3$, and Nb_2O_5 (K:Ca:Nb = 1.1:2:3) at 1473 K for 12 h in air. The obtained powder (5 g) was stirred in 200 cm^3 of a HNO_3 solution (5 M) for 72 h to replace K^+ by H_3O^+. After filtration, the solid was washed with distilled water and then dried in air. The acid-exchanged product was identified to be $HCa_2Nb_3O_{10}\cdot 1.5H_2O$ by X-ray powder diffraction method. A 0.4 g sample of this $HCa_2Nb_3O_{10}\cdot 1.5H_2O$ precursor powder was dispersed in 100 cm^3 of a tetrabutylammonium hydroxide (TBA^+OH^-) aqueous solution with a molar ratio of TBAOH:$HCa_2Nb_3O_{10}\cdot 1.5H_2O$ = 1:2. The mixture was then shaken vigorously at ambient temperature for 4 days. A colloidal suspension, i.e., aggregate of nanosheets of perovskite-type niobate, was finally obtained after removing sediment at the bottom of the flask.

In-Situ TEM Observation. The specimen for TEM examination was prepared by directly dripping droplets of the diluted colloidal suspension onto a carbon-coated Cu microgrid. The in-situ irradiation study was undertaken at room temperature

10.1021/jp0204298 CCC: $25.00 © 2003 American Chemical Society
Published on Web 06/20/2003

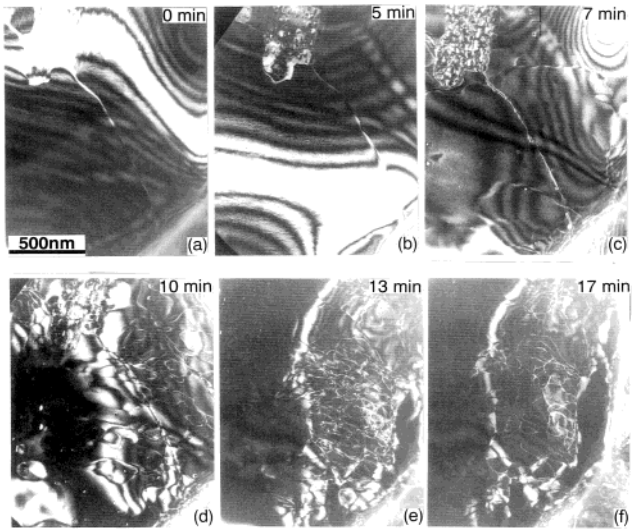

Figure 1. TEM micrographs of an individual nanosheet aggregate undergoing electron irradiation (100 pA/cm^2) at room temperature after progressing time: (a) 0 min, (b) 5 min, (c) 7 min, (d) 10 min, (e) 13 min, (f) 17 min.

on a JEOL3010F field-emission transmission electron microscope (FETEM) operated at 300 kV. A side-entry specimen holder is attached to the microscope with a double-tilting goniometer (±30°). Chemical analysis was performed by energy-dispersive X-ray spectroscopy (EDS) on a spectrometer of EX-14S620N, JEOL. A heating study was performed on the same microscope but with a double-tilting thermal specimen holder. The nanosheet aggregates were dripped on a Mo microgrid. The temperature was increased to 500 °C with a step of 10 °C.

Results and Discussion

Structural Modification upon Electron Irradiation. Exposure of the present niobate nanosheet material to the high-energy electron beams (300 kV) has brought about severe changes of microstructures and formation of a variety of structural defects. Illumination with a mediate electron flux of 100 pA/cm^2 has been found to cause the change. The material is thus very sensitive to the electron illumination, matching the report by Bando et al., who revealed enhanced radiation damage at low temperature for inorganic materials that contain water molecules.[16] Point-defect processes must have meant contribution to the observed structural changes due to the low-temperature migration of point defects induced by electron irradiation.[17] Vacancy is a typical structural defect which exhibits a considerable amount in the present niobate nanosheets.[18] Different effects of electron beams on the hard perovskite and the soft interlayer molecules lead to complicacy of structural features as revealed under the present microscopic observation.

Figure 1a−f and Figure 2a,b show the series of TEM micrographs of two individual nanosheets fragments, recorded at a progressing time sequence under 300 kV electron irradiation with a flux of 100 pA/cm^2 at room temperature. The first structural feature generated upon electron irradiation is found to be the stacking fault pyramids (SFP) or loops. Nucleation-and-growth processes of SFPs and loops are clearly seen in Figure 1a−d and Figure 2, respectively. The athermally radiation-induced diffusion is thus ready to proceed in the present layered perovskite system. Migration of vacancies to a preexisting vacancy cluster (Figure 2a) eventually forms a loop, the collapse of vacancies with disc-shape. The most common

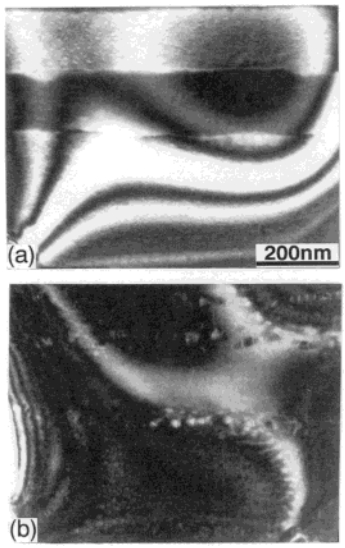

Figure 2. Formation of loops (b) from vacancy clusters (a) under electron irradiation.

structural features that formed under prolonged electron irradiation are domain boundaries. Large numbers of domain boundaries were generated which had initiated from the region covered by the center of electron beams. Under the electron microscope, the movement of these domain boundaries is observed to be quite similar to the diffusion of water waves. The number of domains increased with ongoing irradiation and then decreased by merging of small domains to form larger ones (Figure 1d−f).

Stacking Fault Pyramids and Loops. The diffusion and agglomeration of point defects under high-energy electron irradiation may form different extended defects. Loops and stacking fault tetrahedra (SFT) are the most common extended defects observed in metals and alloys bearing particle irradiation.[19] Loops exhibit very simple structure except for the determination of their nature, i.e., vacancy- or interstitial-type. In our recent paper, a considerable density of vacancies has been revealed in the present niobate nanosheets.[18] The exfoliation process has caused the regional collapse of the perovskite structure, subtracting the number of octahedral layers from three to two in an individual perovskite slab. The preexisting collapsed region exhibits vacancy loop contrast under TEM observation. In this study, the structure of loops created via agglomeration of vacancies under electron irradiation is found similar to that of a collapsed region. Loops are usually parallel to the sheet plane, indicative of the formation of disks of vacancies on the surface of an individual elementary perovskite slab. The final average size of loops is 25 nm.

Compared to the easy cognizance of loops, the formation and the structure of SFPs are fairly amazing for the present perovskite-type material since no SFPs have ever been observed in a bulk perovskite material. Moreover, no reports have ever been available on the formation of SFPs as extended defects under irradiation. Only loops were discovered in the bulk perovskite material under room-temperature irradiation,[15] while SFPs were exclusively observed in the thin films epitaxially grown on a substrate.[20] In the present irradiation study, SFPs may form anywhere but seem more preferably nucleated at the structural defects, e.g., the preexisting antiphase boundary (APB)[18] (Figure 1c). It is noted that the SFPs are evenly spaced at the APB, showing a linear ordering roughly in the [010] direction with an average interval of 100 nm. A similar directional arrangement of SFPs is also found in the matrix as

indicated by a dashed line extending in the [110] direction in Figure 1c. Thus, distribution of SFPs has shown a certain degree of ordering configuration. Ordering of extended defects, e.g., SFTs has been observed in some metals and was interpreted taking into account the anisotropy of the interaction between vacancies and their extended defects.[21] The structure of SFPs observed in the present study has been characterized recently,[22] which shows {111} fault planes and 1/3⟨211⟩ -type displacement.

At the beginning of electron irradiation, the created interstitials may combine with the vacancies that were already present in the structure. This step is equivalent to the diffusion process of vacancies. In the metals and alloys, radiation-induced vacancy migration at low-temperature irradiation has been widely observed.[17,23] Vacancy cluster growth induced by electron irradiation was also found in perovskite-type structures.[15] For the present case, the elementary perovskite sheet is very thin (∼1.2 nm), hence the very short diffusion path to the surface. The abundant surface areas, which act as preexisting sinks, together with the short diffusion path favor the radiation-induced vacancy migration to the surface. The interlayer molecules are soft and flexible, and are assumed to be weakly bonded to the perovskite slabs; thus they have less effect on the point-defect process. Agglomeration of vacancies at the surfaces employed a disk shape that was imaged as a loop. Apparently, the eventual size of loops is highly dependent on the density of the preexisting vacancies. The majority of loops observed in our present study lie on the (001) basal plane. This configuration did not increase the interface area and hence is energetically preferred. Loops on (100) or (010) were also observed but in very small amount.

Unlike the loops, the formation of SFPs must have been related to the interaction with the interlayer species since the well-arranged SFPs agglomerates are involved in several perovskite slabs. SFPs could have been generated in the region where nanosheet aggregates had been dehydrated. This is why fewer domain boundaries were produced during the progressing electron irradiation at the region containing a higher density of SFPs (Figure 1). Domain boundaries formed following the dehydration process as will be cited in the next section. Strong interaction of interlayer atoms with the perovskite layer gives rise to a rigid crystal structure at the expense of loss of surface areas. Collapsing of the vacancy-rich regions into SFP is equivalent to a homogeneous nucleation of SFP on the sites of a primitive perovskite lattice. Formation of SFPs starts from the uppermost layer that is in the immediate vicinity of aggregates surface. The anisotropy of the SFP strain field in one perovskite slab is conveyed to the vacancy fluxes both within the same slab and at the neighboring slab, which is at the present very close to the upper slab. This allowed the rigid vacancy-migration along the ⟨101⟩-oriented stair-rod dislocations. Therefore, it seems that a random and statistical diffusion process similar to the thermally activated jump of point defects will form loops, while a rigid vacancy migration along ⟨101⟩-oriented channels will form SFPs. The formation of SFPs other than SFTs under electron irradiation is reasonable for this specific two-dimensional crystal structure. The layered configuration of roughly cubic perovskite structure tends to be structurally anisotropic. SFTs form only in a rigid isotropic three-dimensional cubic structure, thus they are forbidden in the present material. On the contrary, the SFPs show symmetry identical to that of the host layered structure.

Increasing the dose of electron beam was found to increase the growth rate and density of SFPs. However, the eventual size of SFPs seems to be determined by the irradiation temperature. The maximum size of SFPs is found to be 30 nm under the present room-temperature irradiation. Further electron irradiation will convert the SFPs into loops.[22] The dynamics of radiation-induced SFPs need further study.

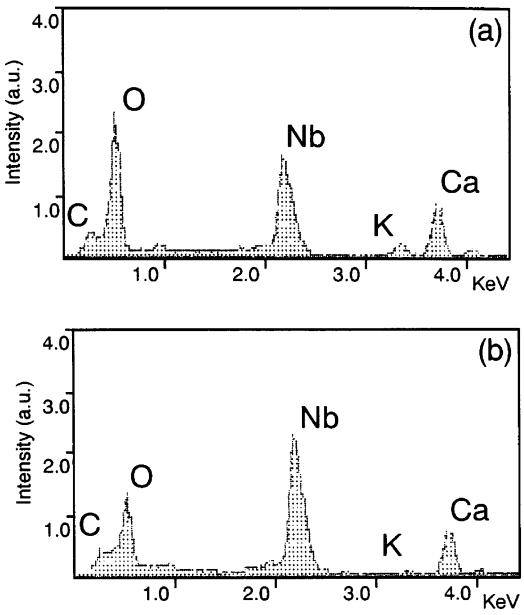

Figure 3. EDS spectra obtained before (a) and after (b) the electron irradiation.

Domain Boundaries. A wide variety of domain boundaries formed under the progress of electron irradiation. Unlike the kinematical effects of electron irradiation that were responsible for the generation of loops and SFPs, the formation of domain boundaries was attributed to the thermal dynamics of electron beams. Thermal dehydration and extraction of soft interlayer TBA molecules that initiated at various sites would form boundaries when they eventually encountered (see Figure 1d−f). A remarkable chemical change has been observed after irradiation as revealed by EDS analysis shown in Figure 3a,b. A decrease in O concentration is quite obvious. The severe loss of oxygen may arise from radiolytic damage in addition to the thermal-induced extraction of interlayer molecules. Meanwhile, the residual potassium atoms have been almost completely removed. The Ca peak also shows decreased peak-area compared to the Nb-peak. This indicates a partial loss of Ca- and O-species via either radiolysis or pyrolysis due to electron illumination. A similar phenomenon has been discovered in $LiNbO_3$ bulk perovskite in which heat treatment would partly remove the Li_2O molecules from the material.[24]

With ongoing electron irradiation, the domain boundaries may either drift when the domains at either side of the boundary differ in composition or structure, or disappear upon coalescence of neighboring domains with identical structure and orientation. The domains are found to exhibit two kinds of crystal structures, i.e., the $HCa_2Nb_3O_{10}$-type structure and superstructures based on it that are created via tilting of octahedra.[25] Continuous electron irradiation will increase the density of the superstructure, indicative of a severe modification of crystal structure induced by the movement of interlayer molecules.

Figure 4 shows the HREM images of different domain boundaries, i.e., (a) nonconservative APB of superlattices, (b) nonconservative APB of basic perovskite structure, (c) δ-boundary, and (d) antiphase boundary exhibiting amorphous interface. Extraction of interlayer molecules must have brought about simultaneous influence on the neighboring perovskite structure.

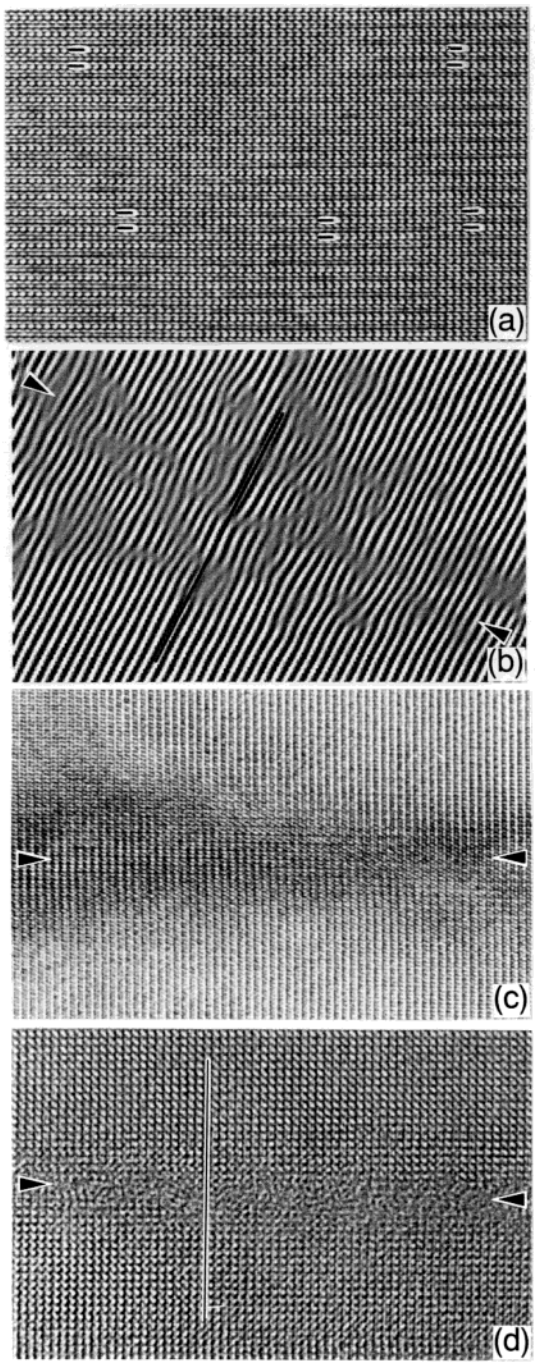

Figure 4. HREM images of (a) a nonconservative APB of superlattice, (b) a nonconservative APB of basic perovskite structure, (c) a δ-boundary, and (d) an APB with amorphous interface.

This is possible for such a thin nanosheet where the atoms are weakly constrained and the bonding structure is very sensitive to the environment. The atoms are highly mobile at high temperatures. For instance, the tilting of rigid octahedra may turn to the opposite direction when the moving interlayer molecules dragged the corners of the octahedra to a certain extent before debonding. Therefore, APBs of superlattices formed as shown in Figure 4a. Neither APBs of superlattice nor APBs of basic perovskite (Figure 4b) showed a conservative configuration. The nonconservative antiphase boundaries suggest atomic displacement other than parallel to the interfaces, indicative of nonthermal-equilibrium process of APB formation, which involved a contribution of point-defect process, e.g., formation of vacancies. The influence of moving interlayer

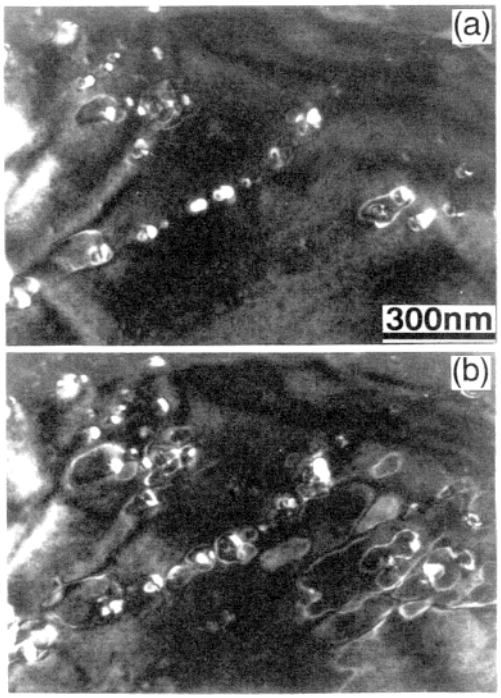

Figure 5. Nucleation (a) and progress (b) of the extraction process near loops.

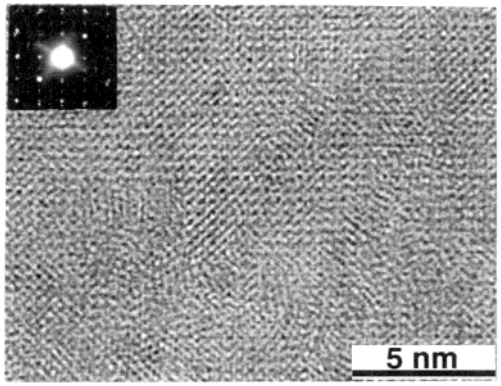

Figure 6. An HREM image and diffraction pattern showing crystal damage after excessive electron irradiation.

molecules on the perovskite structure is at maximum in Figure 4d. Amorphization of local lattice by such process is comparable to the kinematical effects of irradiation damage. Unlike the formation of a transition area at the antiphase boundary during an ion-exchange process,[18] the presence of an amorphous layer at the boundary region may infer high energy of APB and local composition fluctuation, e.g., presence of point-defect clusters.

Dehydration and extraction processes are found to set on preferably near the structural defects. Loops, for example, usually act as the starting point for the extraction process as could be seen in Figure 5a,b. Thermal dynamics of electron illumination enhance the mobility of atoms. The extraction process involves debonding of interlayer molecules from the perovskite. The structural imperfection has weakened the local chemical bonds due to the lack of a rigid crystal-field potential. In the region of loops, the interlayers expanded, hence a decreased bonding strength of molecules to the nanosheets. It could be seen that the density of domain boundaries depends on the number of nucleation sites for the extraction process. Consequently, a high density of preexisting defects in the structure will eventually result in an increased number of domain boundaries.

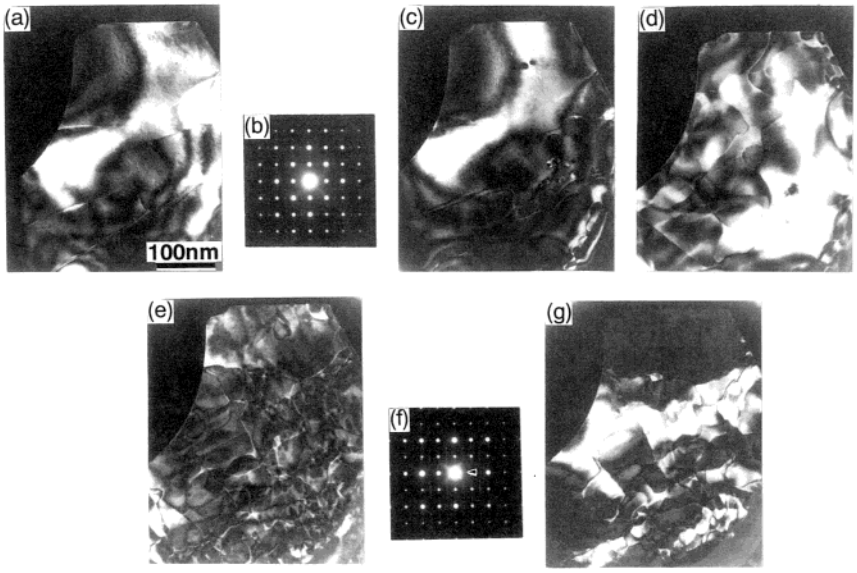

Figure 7. Series of micrographs obtained in heating process with duration of 5 min at each temperature: (a) 22 °C, (c) 110 °C, (d) 150 °C, (e) 190 °C, (g) 405 °C. (b) and (f) show diffraction patterns obtained before and after heating, respectively.

Further electron irradiation would not change the structures of loops and domain boundaries but would cause crystal damages. The HREM image and electron diffraction in Figure 6 illustrate the tendency of polycrystallization and amorphization. Thus, the electron irradiation on nanosheet aggregates is a complicated process involving the combination of kinematical and thermal dynamic effects.

Structural Modification upon Heating. To investigate the pure effects of heating on the structures, we decreased the filament current during the TEM observation to avoid possible contribution from electron irradiation. Figure 7 shows the series of micrographs recorded at different increasing temperatures. At a temperature slightly above 100 °C, bubbles formed as the nucleation sites for extraction. The bubbles did not live long and soon disappeared. It is noted that the boundaries preexisting in the structure started to move at this temperature (Figure 7c). The boundaries drifted and their shapes changed correspondingly. Some boundaries show separated double-line contrast and the interval of the separated boundaries was expanding. The preexisting boundaries in Figure 7a were identified as APB with regard to the basic perovskite structure. As has been cited in our previous work, the antiphase boundaries involve a transition width of two or three octahedra.[18] This suggests high formation energy of APBs in the present system. Thus, APBs are metastable and are ready to drift after activation energy is favored by heating. The separation of APBs is due to different movement of the antiphase boundary at different elementary nanosheets along the depth of aggregates.

By increasing the temperature to 150 °C, the extraction process was initiated from the edges of nanosheet aggregates (Figure 7d). The boundary contrast from different interlayers moved inward. The following extraction of interlayer molecules at increased temperatures was similar to the thermodynamic process of electron irradiation. A variety of domain boundaries formed, merged, and eventually were stabilized in a certain configuration. Further heating would not annihilate the domain boundaries.

Compared to the thermal dynamics of electron irradiation, heating exhibits the initiation of extraction exclusively from the edges of nanosheet aggregates. The extraction process was going on with a simultaneous change in electron diffraction, as shown in Figure 7b,f. Though it did not show so extreme changes as

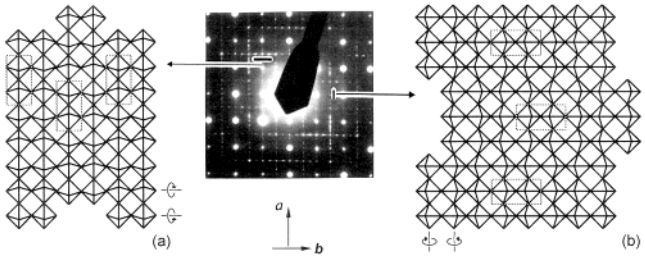

Figure 8. Ideal periodic antiphase domain boundaries on (a) (010) and (b) (100) planes. Different periodicities are revealed by the attached diffraction pattern.

electron irradiation did, heating involved a synchronous reaction of the entire system while electron irradiation only brought about local modification. Streaks penetrating the superlattice reflections along ⟨100⟩ axes indicate the presence of small periodic antiphase domains in the extracted structure. Streaks are always perpendicular to the corresponding superlattice reflection vectors. For example, the streak penetrating the (0, 1/2, 0) superlattice spot (arrowed in Figure 7f) extends along the [100] direction. This indicates alignment of well-defined antiphase domains in the direction normal to the superlattice dimension. The domains are bounded by (100) planes and show narrow width in the [100] alignment direction. Two ideal structural models of periodic antiphase domain boundaries are schematically illustrated in Figure 8a,b for ordering in the *b* and *a* directions, respectively. The unit cell of superstructure due to tilting of octahedra along a tetrad in the same direction of ordering is outlined in each model. The experimental selected-area diffraction pattern in the middle corresponds well to each of the proposed models that show 2-fold and 3-fold periodicity along the domain width. The crystal structure at either side of the APB is identical except for a lattice shift of one octahedron, i.e., half of the superlattice dimension, parallel to the boundary. The width of antiphase domains is well defined for each model, i.e., two and three octahedra for Figure 8a and 8b, respectively. Periodic APB structure is a typical feature observed in every nanosheet aggregate after heating. APBs of superlattice were also discovered during electron irradiation as has been shown in Figure 4a. However, in that case, the majority of antiphase domains applied to a long-range ordering configuration, which did not show any satellite reflections on the electron diffraction

pattern (Figure 6b). The difference in APB configuration between the electron irradiation and the heating process is still not well understood. It may probably arise from the difference in the number of nucleation sites and/or the growth rate of antiphase domain boundaries. The temperature and the formation energies of APBs on different crystallographic faces might have to be taken into account. The present in-situ TEM observation did not find any evidence of massive movement of perovskite layers during heating. In the heating process, extended defects, e.g., loops and SFPs created in a point-defect process could not be observed.

Conclusions

Effects of electron irradiation and heating on the novel perovskite-type niobate nanosheet aggregates have been studied via an in-situ TEM observation. A radiation-induced migration of vacancies at room temperature has been observed which eventually brought about the formation of loops and stacking fault pyramids. The thermodynamic and radiolytic effects of electron irradiation have caused partial loss of Ca- and O-species and generated a variety of domain boundaries, the products of extraction of interlayer molecules. Similar domain boundaries have also been produced after heating. However, heating has shown short-range ordering by forming periodic antiphase domains while thermal dynamics of electron irradiation were in favor of domain configuration typical of long-range ordering.

Acknowledgment. The authors are grateful to Mr. K. Kurashima in NIMS for help with experimental work.

References and Notes

(1) Jacobson, A. J. *J. Mater. Sci. Forum* **1994**, *152*−*153*, 1.

(2) (a) Sasaki, T.; Watanabe, M.; Hashizume, H.; Yamada, H.; Nakazawa, H. *J. Am. Chem. Soc*. **1996**, *118*, 8329. (b) Sasaki, T.; Watanabe, M. *J. Am. Chem. Soc*. **1998**, *120*, 4682. (c) Sasaki, T.; Watanabe, M.; Michiue, Y.; Komatsu, Y.; Izumi, F.; Takenouchi, S. *Chem. Mater*. **1995**, *7*, 1001. (d) Sasaki, T.; Kooli, F.; Iida, M.; Michiue, Y.; Takenouchi, S.; Yajima, Y.; Izumi, F.; Chakoumakos, B. C.; Watanabe, M. *Chem. Mater*. **1998**, *10*, 4123. (e) Sukpirom, N.; Lerner, M. M. *Chem. Mater*. **2001**, *13*, 2179.

(3) (a) Jacobson, A. J.; Lewandowski, J. T.; Johnson, J. W. *J. Less Common Met*. **1986**, *116*, 137. (b) Treacy, M. M. J.; Rice, S. B.; Jacobson, A. J.; Lewandowski, J. T. *Chem. Mater*. **1990**, *2*, 279. (c) Schaak, R. E.; Mallouk, T. E. *Chem. Mater*. **2000**, *12*, 2513. (d) Schaak, R. E.; Mallouk, T. E. *Chem. Mater*. **2000**, *12*, 3434. (e) Han, Y. S.; Park, I.; Choy, J. H. *J. Mater. Chem*. **2001**, *11*, 1277.

(4) (a) Sasaki, T.; Watanabe, M. *J. Phys. Chem. B* **1997**, *101*, 10159. (b) Sasaki, T.; Ebina, Y.; Watanabe, M.; Decher, G. *Chem. Commun*. **2000**, 2163.

(5) Ebina, Y.; Sasaki, T.; Watanabe, M. *Solid State Ionics*, submitted.

(6) (a) Otzschi, K. D.; Poeppelmeier, K. R.; Salvador, P. A.; Mason, T. O.; Zhang, H.; Marks, L. D. *J. Am. Chem. Soc*. **1996**, *118*, 8951. (b) Salvador, P. A.; Greenwod, K. B.; Mawdsley, J. R.; Poeppelmeier, K. R.; Mason, T. O. *Chem. Mater*. **1999**, *11*, 1760.

(7) (a) Brahmaroutu, B.; Messing, G. L.; Trolier-Mckinstry, S.; Selvaraj, U. In *Proceedings of the 10th IEEE International Symposium on Applications of Ferroelectrics, Vol II*; Kulwicki, B. M., Amin, A., Safari, A., Eds.; IEEE: Piscataway, NJ, 1996; pp 883−886. (b) Takeuchi, T.; Tani, T.; Satoh, T. *Solid State Ionics* **1998**, *108*, 67. (c) Horn, J.; Zhang, S. C.; Selvaraj, U.; Messing, G. L.; Trolier-Mckinstry, S. *J. Am. Ceram. Soc*. **1999**, *82*, 921. (d) Rehrig, P. W.; Park, S.-E.; Trolier-Mckinstry, S.; Messing, G. L.; Jones, B.; Shrout, T. R. *J. Appl. Phys*. **1999**, *86*, 1657.

(8) (a) Takata, T.; Furumi, Y.; Shinohara, K.; Tanaka, A.; Hara, M.; Kondo, J. N.; Domen, K. *Chem. Mater*. **1997**, *9*, 1063. (b) Kim, H. G.; Hwang, D. W.; Kim, J.; Kim, Y. G.; Lee, J. S. *Chem. Commun*. **1999**, 1077.

(9) Moritomo, Y.; Asamitsu, A.; Kuwahara, H.; Tokura, Y. *Nature* **1996**, *380*, 141.

(10) Yanagisawa, O.; Izumi, M.; Huang, K. H.; Hu, W. Z.; Shen, Y.; Nakanishi, K.; Takahashi, Y.; Nojima, H. *J. Magn. Magn. Mater*. **2000**, *211*, 133.

(11) Mitchell, J. N.; Yu, N.; Sickafus, K. E.; Nastasi, M. A.; McClellan, K. J. *Philos. Mag. A* **1998**, *78*, 713.

(12) Scacco, A.; Furetta, C.; Bacci, C.; Ramogida, G.; Sanipoli, C. *Nucl. Instrum. Meth. B* **1994**, *91*, 223.

(13) Xiong, S. B.; Ye, Z. M.; Liu, J. M.; Li, A. D.; Lin, C. Y.; Chen, X. Y.; Guo, X. L.; Liu, Z. G. *Appl. Surf. Sci*. **1997**, *110*, 124.

(14) Ball, C. J.; Blake, R. G.; Cassidy, D. J.; Woolfrey, J. L. *J. Nucl. Mater*. **1988**, *151*, 151.

(15) Buck, E. C. *Radiat. Eff. Defects Solids* **1995**, *133*, 15.

(16) Bando, Y.; Kitami, Y.; Yokoyama, M. In *Proceedings of the 12th International Congress in Electron Microscopy*, 1990; pp 806−807.

(17) Urban, K.; Seeger, A. *Philos. Mag*. **1974**, *24*, 1395.

(18) Xu, F. F.; Ebina, Y.; Bando Y.; Sasaki, T. *J. Phys. Chem. B*, submitted.

(19) (a) Ruault, M. O.; Jouffrey, B. *Appl. Phys. Lett*. **1974**, *25*, 265. (b) Yoshida, N.; Kiritani, M. *J. Phys. Soc. Jpn*. **1975**, *38*, 1220. (c) Urban, K.; Jäger, W. *Phys. Status Solidi B* **1975**, *68*, K1. (d) Fujita, H.; Sakata, T.; Fukuyo, H. *Jpn. J. Appl. Phys*. **1982**, *21*, L235.

(20) (a) Kakibayashi, H.; Nagata, F.; Katayama, Y.; Shiraki, Y. *Jpn. J. Appl. Phys*. **1984**, *23*, L846. (b) Lee, J. D.; Park, J. C.; Venables, D.; Krause, S. J.; Roitman, P. *Appl. Phys. Lett*. **1993**, *63*, 3330. (c) Wang, N.; Sou, I. K.; Fung, K. K. *Philos. Mag. Lett*. **1997**, *76*, 153. (d) Kasai, J. I.; Kawata, M. *Appl. Phys. Lett*. **1998**, *73*, 2012.

(21) (a) Kubin, L.; Rocher, A.; Ruault, M. O.; Jouffrey, B. *Philos. Mag*. **1976**, *23*, 293. (b) Jin, N. Y.; Phillipp, F.; Seeger, A. *Phys. Status Solidi A* **1989**, *116*, 91. (c) Seeger, A.; Jin, N. Y.; Phillipp, F.; Zaiser, M. *Ultramicroscopy* **1991**, *39*, 342. (d) Tölg, C.; Zaiser, M.; Hähner, P.; Frank, W. *Appl. Phys. A* **1994**, *A58*, 3.

(22) Xu, F. F.; Bando Y.; Ebina, Y.; Sasaki, T. *Philos. Mag. Lett*., in press.

(23) (a) Ding, F. R.; Averback, R. S.; Hahn, H. *J. Appl. Phys*. **1988**, *64*, 1785. (b) Dajello, P. C. T.; Scherer, C. *J. Phys. D* **1992**, *25*, 1780. (c) Hashimoto, T.; Isobe, Y.; Shigenaka, N. *Mater. Trans., JIM* **1995**, *36*, 639. (d) Schule, W. *Z. Metallkd*. **2000**, *91*, 728.

(24) Holman, R. L.; Cressman, P. J.; Revelli, J. F. *Appl. Phys. Lett*. **1978**, *32*, 280.

(25) Xu, F. F.; Bando Y.; Ebina, Y.; Sasaki, T. *Philos. Mag. A*. **2002**, *82*, 2655.